Inorganic Chemistry

ARTICLE

pubs.acs.org/IC

Phase Transitions of $AlFeO_3$ and $GaFeO_3$ from the Chiral Orthorhombic ($Pna2_1$) Structure to the Rhombohedral ($R\bar{3}c$) Structure

Rana Saha, Ajmala Shireen, Sharmila N. Shirodkar, Mukta Shashi Singh, Umesh V. Waghmare, A. Sundaresan, and C. N. R. Rao*

Chemistry and Physics of Materials Unit, New Chemistry Unit, Theoretical Science Unit and International Centre for Materials Science, Jawaharlal Nehru Centre for Advanced Scientific Research, Jakkur, Bangalore 560064, India

ABSTRACT: $AlFeO_3$ and $GaFeO_3$, which crystallize in a chiral orthorhombic ($Pna2_1$) structure, transform to a rhombohedral ($R\bar{3}c$) structure when subjected to ball-milling. There is a distinct difference between the transformations of $AlFeO_3$ and $GaFeO_3$. $AlFeO_3$ first transforms to an orthorhombic $P2_12_12_1$ structure followed by its transformation to the $R\bar{3}c$ structure, while $GaFeO_3$ goes directly to the $R\bar{3}c$ structure. The transformations have been characterized by X-ray diffraction and Raman spectroscopy. Magnetic properties of $Pna2_1$ and the transformed phases show significant differences. It is noteworthy that partial substitution of aluminum by gallium in $AlFeO_3$ as in $Al_{0.5}Ga_{0.5}FeO_3$ eliminates the intermediate $P2_12_12_1$ phase, causing direct transformation of the $Pna2_1$ structure to the $R\bar{3}c$ structure. All of the transformations are thermodynamically first-order associated with significant changes in volume. We have used first-principles simulations to determine the pressure-dependent properties of $AlFeO_3$ and $GaFeO_3$ in orthorhombic and corundum structures and have estimated the critical pressures for the structural phase transition between the two structures. On the basis of this information, we also comment on the differences in the behavior of $AlFeO_3$ and $GaFeO_3$ under ball-milling.

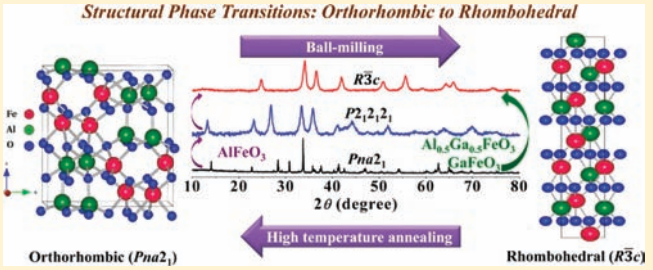

INTRODUCTION

$AlFeO_3$ and $GaFeO_3$ are members of a family of oxides with interesting dielectric and magnetic properties.[1−3] Interestingly, $AlFeO_3$ and $GaFeO_3$ crystallize in the chiral orthorhombic structure ($Pna2_1$),[4] although the component oxides possess different structures. Both α-Al_2O_3 and α-Fe_2O_3 crystallize in the rhombohedral structure ($R\bar{3}c$), while β-Ga_2O_3 has a monoclinic structure ($C2/m$). $GaFeO_3$ has been reported to be piezoelectric and ferromagnetic.[5] It has been shown recently that members of the $Al_{1-x}Ga_xFeO_3$ family exhibit significant magnetodielectric effects.[6,7] There has been some interest in investigating the phase transitions of these oxides. Studies of $AlFeO_3$ and $GaFeO_3$ at high pressures and high temperatures seem to indicate the occurrence of decomposition, while there are also reports of a transition to the perovskite phase at high pressure.[8,9] The studies of Nagai et al.,[10] although not entirely clear, seem to suggest that the structure of $AlFeO_3$ transforms to another form of the orthorhombic structure at high pressures and comes back to the trigonal phase upon release of the pressure. We were interested in exploring the phase transitions of $AlFeO_3$ and $GaFeO_3$ because of their unique structures and properties, especially to find out whether the chiral orthorhombic structures of these oxides transform to other structures when subjected to grinding or ball-milling. To our surprise, we find that ball-milling transforms these oxides from the chiral orthorhombic structure ($Pna2_1$) to the rhombohedral structure ($R\bar{3}c$), with significant differences between $AlFeO_3$ and $GaFeO_3$ with regard to the nature of the transformation. Besides characterizing the phase transitions by X-ray diffraction (XRD) and Raman spectroscopy, we have studied the magnetic properties of the different phases. We have also carried out first-principles calculations to understand the nature of the phase transitions.

EXPERIMENTAL SECTION

$AlFeO_3$, $GaFeO_3$, and $Al_{0.5}Ga_{0.5}FeO_3$ were prepared by the coprecipitation method or solid-state reaction starting with stoichiometric amounts of α-Fe_2O_3 (Aldrich, 99.98%), α-Al_2O_3 (Alfa-Aesar, 99.99%), and β-Ga_2O_3 (Aldrich, 99.99%). Fe_2O_3 and $Al(Ga_2O_3)$ powders were dissolved separately in concentrated HCl to form the chlorides; the metal chloride solutions were mixed and stirred for 0.5 h, after which a NH_4OH solution was added dropwise with continuous stirring until precipitation. The precipitate was filtered, washed with distilled water to remove residual ammonium chloride salt until neutral pH was attained, and dried at 80 °C in an air oven for 24 h. The dried precipitates were heated at 1350 °C for 2 h in air with a heating rate of 3 °C/min. These compounds were also made by conventional solid-state reactions where in mixtures of the component oxides were heated at 1400 °C with repeated grinding, pelletizing, and heating. These oxides were subjected to ball-milling using a planetary monomill (Fritsch Pulverisette-6, Berlin, Germany). A batch of 2 g of each sample was taken separately in a 80 mL capacity agate (99.9% SiO_2) bowl containing 10−15 agate balls of 10 mm

Received: June 9, 2011
Published: August 26, 2011

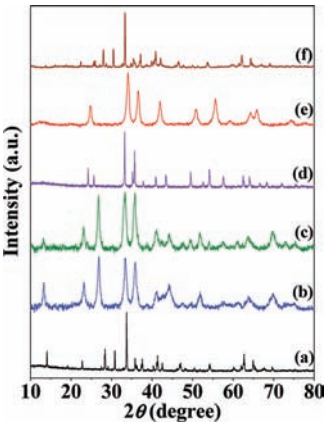

Figure 1. XRD patterns of (a) the orthorhombic $AlFeO_3$ sample, (b) ball-milled $AlFeO_3$ (12 h), (c) 12 h ball-milled $AlFeO_3$ annealed at 700 °C, (d) a mixture of α-Fe_2O_3 + α-Al_2O_3 (1:1), (e) ball-milled $AlFeO_3$ (24 h), and (f) 24 h ball-milled $AlFeO_3$ annealed at 1350 °C, with the $Pna2_1$ space group.

diameter. Ball-milling was carried out without any additives (dry ball-milling) at a speed of 400 rpm for 12−24 h. The ambient temperature during ball-milling was around 400 °C. It is important to note that no contamination was found in the ball-milled samples from the ball-milled vessel. The ball-milled samples were subjected to various methods of characterization. They were also annealed in air at 700 °C, and the annealed samples were characterized similarly. The annealed samples were also heated to 1000−1350 °C in air for a period of 24 h.

XRD patterns of the powdered samples were recorded with a Bruker D8 Advance X-ray diffractometer to confirm the phase purities of these oxides. The software package *Fullprof* was used to analyze the structural data. Raman spectra of powdered samples were recorded at room temperature with a LabRAM HR 800 high-resolution Raman spectrometer (Horiba-Jobin Yvon) using a He−Ne laser (λ = 632.8 nm). Magnetic properties of the samples were measured using a vibrating sample magnetometer in the Physical Property Measurement System (PPMS) under zero-field-cooled (ZFC) and field-cooled (FC) conditions in the temperature range of 5−390 K under a magnetic field of 100 Oe. Magnetic hysteresis curves were recorded at 5 K in magnetic fields going up to 60 kOe.

We have carried out first-principles calculations to examine the pressure dependence of the $Pna2_1$ and $R\bar{3}c$ structures of $AlFeO_3$ and $GaFeO_3$. The calculations are based on density functional theory (DFT) with a spin-density-dependent exchange correlation energy functional of a generalized gradient approximation [Perdew−Wang 91 (PW 91)] form[11] as implemented in the Vienna Ab initio Simulation Package.[12,13] The projector augmented wave method[14] is used to capture the interaction between ionic cores and valence electrons. An energy cutoff of 400 eV was used for the plane-wave basis, and integrations over the Brillouin were sampled upon using a regular 4 × 2 × 2 mesh of k points for the orthorhombic structure and a 3 × 3 × 2 mesh for the corundum structure. The pressure dependence of these structures was studied by homogeneously deforming the unit cell by up to ±2% isotropic strain and obtaining the corresponding pressure from the stress tensor calculated as a derivative of the energy with respect to strain. To determine the critical pressure, we define an enthalpy $H = E(V) + PV$, where $E(V)$ is the total energy function of a parabolic form fitted to energies obtained in the DFT calculations and V is the volume of the unit cell. For a given pressure, the equilibrium volume is obtained by minimizing H with respect to V. The critical pressure is the pressure at which the minimum enthalpies of the two structures cross, which also relates to the slope of a common tangent to the energy−volume curves of two structures.

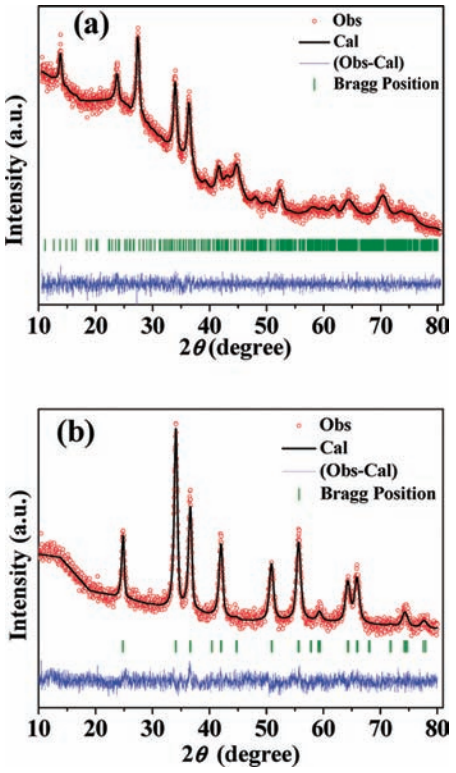

Figure 2. XRD patterns of ball-milled $AlFeO_3$ in (a) the δ-Al_2O_3 structure ($P2_12_12_1$) and (b) the $R\bar{3}c$ structure along with profile fits, difference patterns, and Bragg positions.

RESULTS AND DISCUSSION

$AlFeO_3$ samples, subjected to ball milling at 300 K for a period of 12 h, were investigated by XRD and Raman spectroscopy. The XRD patterns of the starting material and of the ball-milled sample are shown in parts a and b of Figure 1, respectively. The ball-milled sample shows line broadening, and the crystallite size calculated from the line width is ∼20 nm. Annealing the ball-milled sample at 700 °C showed no changes in the positions of the reflections, as can be seen from Figure 1c. The XRD pattern of the ball-milled $AlFeO_3$ does not match that of α-Fe_2O_3. Furthermore, a 1:1 mixture of α-Fe_2O_3 and α-Al_2O_3 exhibits a XRD pattern (Figure 1d) that is completely different from that of ball-milled $AlFeO_3$. Profile fitting using the *Fullprof* package (Figure 2a) showed that the structure of ball-milled $AlFeO_3$ was akin to δ-Al_2O_3 with the $P2_12_12_1$ space group.[15] The lattice parameters of this $P2_12_12_1$ were found to be a = 15.886 (11) Å, b = 11.408 (6) Å, and c = 7.803 (4) Å. The δ-Al_2O_3 phase is related to the spinel structure and is different from that of δ*-Al_2O_3 ($P222$)[16] with lattice parameters a = 7.936 Å, b = 7.956 Å, and c = 11.711 Å reported by Fargeot et al.[16] It is, however, difficult to differentiate the $P222$ and $P2_12_12_1$ structures based on profile fitting. It is possible that the δ* phase of Fargeot et al.[16] is actually the δ phase described by Levin and Brandon.[15]

In order to examine whether ball-milling for extended periods gives rise to other structures, we ball-milled $AlFeO_3$ for 24 h at 300 K. The XRD pattern of this sample (Figure 1e) is similar to that of α-Fe_2O_3 ($R\bar{3}c$). The lattice parameters of the rhombohedral $AlFeO_3$ are a = 4.909(2) Å and c = 13.393(7) Å, as obtained from profile fitting (Figure 2b). Note that the lattice parameters of α-Fe_2O_3 are a = 5.032 Å and c = 13.733 Å, while those of

dx.doi.org/10.1021/ic201235h |*Inorg. Chem.* 2011, 50, 9527–9532

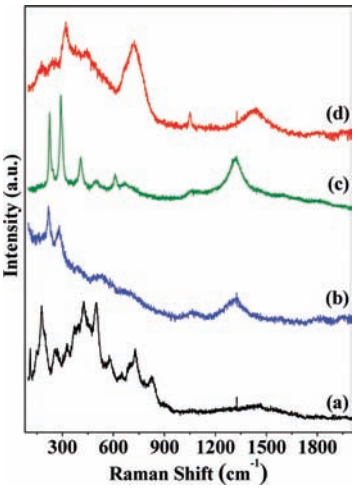

Figure 3. Raman spectra of (a) the orthorhombic $AlFeO_3$ sample, (b) ball-milled $AlFeO_3$ (12 h), (c) 12 h ball-milled $AlFeO_3$ annealed at 700 °C, and (d) ball-milled $AlFeO_3$ (24 h).

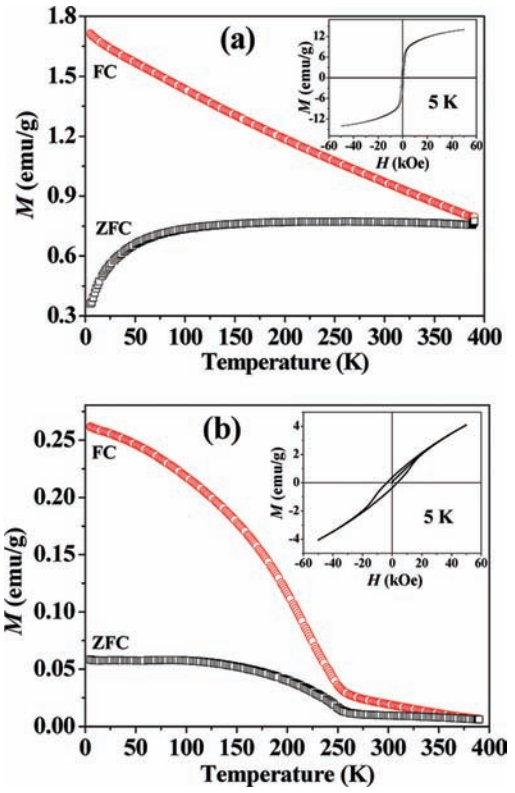

Figure 4. Temperature-dependent magnetization of ball-milled $AlFeO_3$ in the (a) $P2_12_12_1$ and (b) $R\bar{3}c$ structures under FC and ZFC conditions. Magnetic hysteresis at 5 K is shown in the inset.

α-Al_2O_3 are a = 4.760 Å and c = 12.993 Å (JCPDS). The $R\bar{3}c$ sample of $AlFeO_3$ transforms to the $Pna2_1$ structure upon heating to 1350 °C, as shown in Figure 1f.

The Raman spectrum of $AlFeO_3$ ball-milled for 12 h at 300 K with the $P2_12_12_1$ structure is distinctly different from that of bulk $AlFeO_3$ with the $Pna2_1$ structure (see Figure 3a,b). After annealing ball-milled $AlFeO_3$ at 700 °C, the Raman spectrum did not change significantly (Figure 3c) except for sharpening of

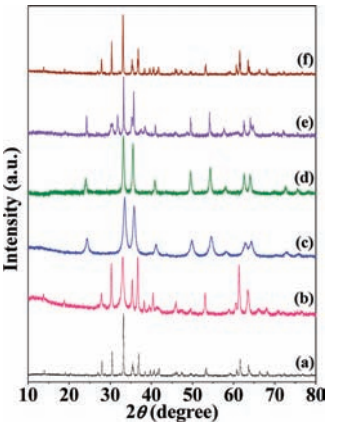

Figure 5. XRD patterns of (a) the orthorhombic $GaFeO_3$ sample, (b) $GaFeO_3$ nanoparticles by the sol−gel route, (c) ball-milled $GaFeO_3$, (d) ball-milled $GaFeO_3$ annealed at 700 °C, (e) a mixture of Fe_2O_3 + Ga_2O_3 (1:1), and (f) ball-milled $GaFeO_3$ annealed at 1000 °C.

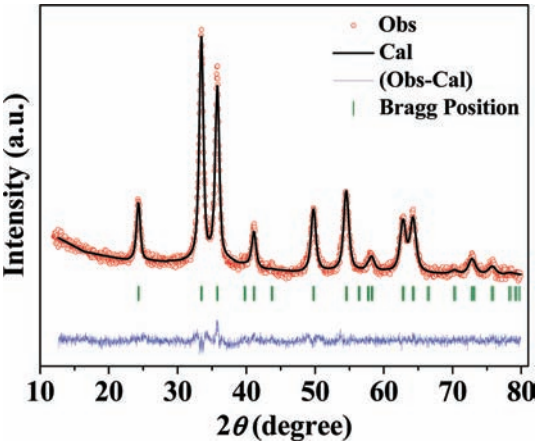

Figure 6. XRD patterns of ball-milled $GaFeO_3$ along with the profile fit, difference pattern, and Bragg positions.

the bands. Figure 3d shows the Raman spectrum of $AlFeO_3$ ball-milled for 24 h at 300 K. The spectrum is as expected for the $R\bar{3}c$ space group. Thus, XRD and Raman studies of $AlFeO_3$ clearly establish that the chiral orthorhombic structure ($Pna2_1$) first transforms to the orthorhombic $P2_12_12_1$ structure of δ-Al_2O_3 upon ball-milling for a period of 12 h and transforms to the rhombohedral $R\bar{3}c$ structure upon further ball-milling. We have carried out direct-current magnetization measurements to establish the magnetic behavior of $AlFeO_3$ with different structures. Magnetization data of $AlFeO_3$ ball-milled for 12 h were compared with those of the $AlFeO_3$ structure with the $Pna2_1$ space group. In Figure 4a, temperature-dependent magnetization data of FC and ZFC of ball-milled $AlFeO_3$ in the $P2_12_12_1$ structure are shown. We observe divergence between the FC and ZFC data below 390 K in the $P2_12_12_1$ sample. Furthermore, the nature of the magnetization curves of this sample is quite different from that of the $Pna2_1$ sample, which shows a sharp ferrimagnetic transition (T_N) at 250 K.[2−4,6] The $P2_12_12_1$ sample shows magnetic hysteresis at 5 K, as shown in the inset of Figure 4a. Figure 4b shows the magnetization data of $AlFeO_3$ in the $R\bar{3}c$ structure obtained by ball-milling for 24 h. The FC data show a

dx.doi.org/10.1021/ic201235h |*Inorg. Chem.* 2011, 50, 9527–9532

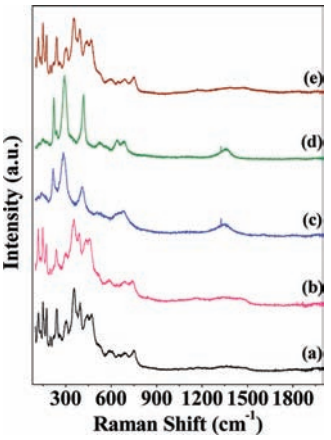

Figure 7. Raman spectra of (a) the orthorhombic $GaFeO_3$ sample, (b) $GaFeO_3$ nanoparticles by the sol−gel route, (c) ball-milled $GaFeO_3$, (d) ball-milled $GaFeO_3$ annealed at 700 °C, and (e) ball-milled $GaFeO_3$ annealed at 1000 °C.

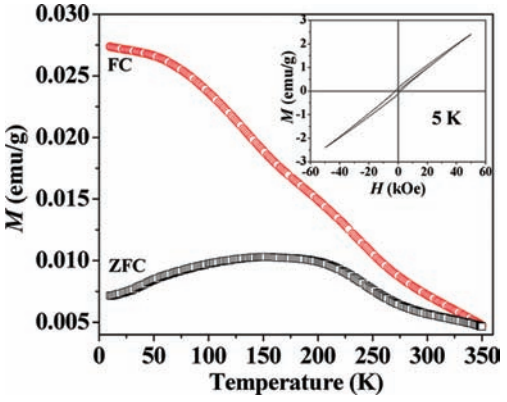

Figure 8. Temperature-dependent magnetization of ball-milled $GaFeO_3$ under FC and ZFC conditions. Magnetic hysteresis at 5 K is shown in the inset.

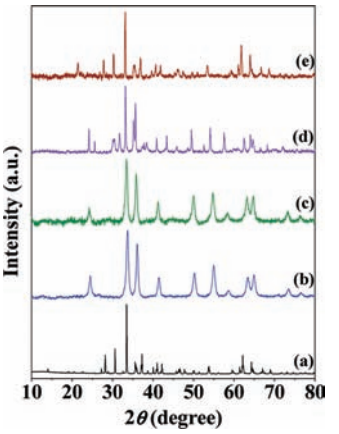

Figure 9. XRD patterns of (a) the orthorhombic $Al_{0.5}Ga_{0.5}FeO_3$ sample, (b) ball-milled $Al_{0.5}Ga_{0.5}FeO_3$, (c) ball-milled $Al_{0.5}Ga_{0.5}FeO_3$ annealed at 700 °C, (d) a mixture of $Fe_2O_3 + Al_2O_3 + Ga_2O_3$ (1:0.5:0.5), and (e) ball-milled $Al_{0.5}Ga_{0.5}FeO_3$ annealed at 1200 °C.

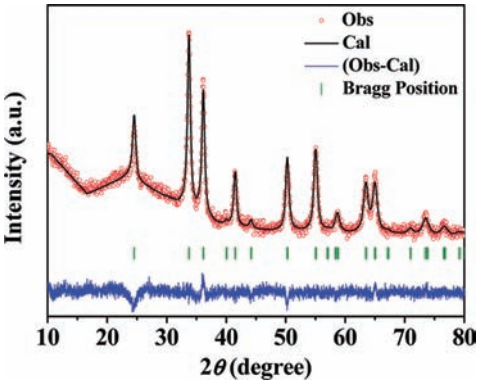

Figure 10. XRD pattern of ball-milled $Al_{0.5}Ga_{0.5}FeO_3$ in the $R\bar{3}c$ structure along with the profile fit, difference pattern, and Bragg positions.

ferrimagnetic transition at a different temperature from that of the $Pna2_1$ structure, with T_N of 225 K. We observe magnetic hysteresis at 5 K in the $R\bar{3}c$ sample as well but no saturation. The magnitudes of magnetization of both the $P2_12_12_1$ and $R3\bar{c}$ samples are much lower than that of the chiral orthorhombic $Pna2_1$ structure, showing a preponderance of antiferromagnetic interaction in these transformed phases.

We next examined the effect of ball-milling on the structure and magnetic properties of $GaFeO_3$. XRD patterns of $GaFeO_3$ in the $Pna2_1$ structure as well as of the $GaFeO_3$ ball-milled for 12 or 6 h at 300 K are shown in Figure 5. The XRD pattern of $GaFeO_3$ nanoparticles prepared by the sol−gel route is also shown in this figure. The XRD pattern of the nanoparticles prepared by the sol−gel route is the same as that of the $Pna2_1$ $GaFeO_3$ (see Figure 5a,b) except for line broadening due to the small size. Using the Debye−Scherrer formula, the particle size was found to be 25 nm. The XRD pattern of ball-milled $GaFeO_3$ (Figure 5c) is quite different from that of the starting material (Figure 5a) and could be readily indexed on the basis of the rhombohedral unit cell ($R\bar{3}c$). The pattern has rather broad reflections due to the small particle size, estimated to be 20 nm. Furthermore, the XRD pattern of a 1:1 mixture of Fe_2O_3 and Ga_2O_3 (Figure 5e) is completely different from that of ball-milled $GaFeO_3$. Upon annealing of the ball-milled $GaFeO_3$ at 700 °C, the XRD pattern remains the same (Figure 5d) but with smaller line width due to the increase in the crystallite size (estimated to be 40 nm). The XRD pattern of ball-milled $GaFeO_3$ is shown along with the profile fit and difference pattern in Figure 6. The lattice parameters of ball-milled $GaFeO_3$ are a = 5.022(2) Å and c = 13.606(5) Å. Note that the lattice parameters of α-Fe_2O_3 and rhombohedral Ga_2O_3 are a = 5.032 Å, c = 13.733 Å and a = 4.979 Å, c = 13.429 Å, respectively. Interestingly, upon heating of the ball-milled $GaFeO_3$ sample to 1000 °C, it transformed back to the orthorhombic chiral ($Pna2_1$) structure, as can be seen from the XRD pattern in Figure 5f.

The Raman spectrum of ball-milled $GaFeO_3$ ($R\bar{3}c$) is compared with that of the chiral orthorhombic sample as well as that of the nanoparticles of $GaFeO_3$ synthesized by the sol−gel route. The Raman spectrum of the starting $GaFeO_3$ sample (Figure7a) is similar to that of the nanoparticles of $GaFeO_3$ (Figure 7b), but we see distinct differences in the spectrum of ball-milled $GaFeO_3$ (Figure 7c). After annealing of the ball-milled $GaFeO_3$ at 700 °C, the spectrum remained the same (Figure 7d) except for sharpening of the bands. The Raman spectrum recorded after annealing of the ball-milled sample at 1000 °C (Figure 7e) is similar to that of the starting $GaFeO_3$ sample (Figure 5a). The XRD and Raman

dx.doi.org/10.1021/ic201235h |*Inorg. Chem.* 2011, 50, 9527–9532

results clearly show that chiral orthorhombic $GaFeO_3$ ($Pna2_1$) transforms directly to the rhombohedral $R\bar{3}c$ structure when subjected to ball-milling, unlike $AlFeO_3$, which goes through an intermediate phase of the $P2_12_12_1$ space group. The space group $R\bar{3}c$, rather than $R3c$, was confirmed by the absence of second harmonic generation by the material.

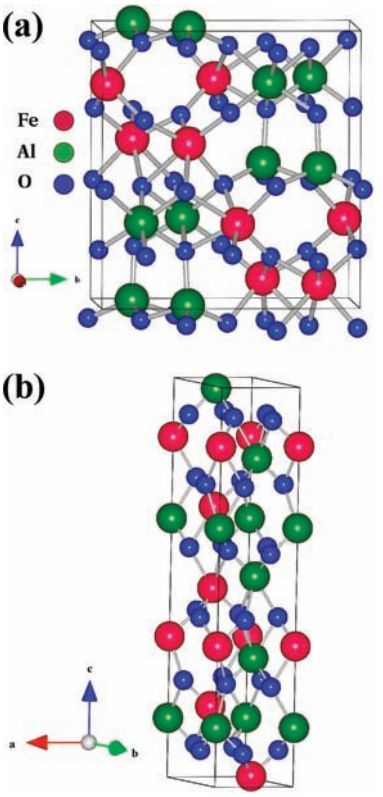

Figure 11. Crystal structures of $AlFeO_3$ in (a) orthorhombic and (b) corundum structures.

Table 1. Structural Data of the Various Phases of $Al_{1-x}Ga_xFeO_3$ (x = 0, 0.5, 1)

structure	space group	a (Å)	b (Å)	c (Å)	R_{Bragg} (%)
		$AlFeO_3$			
orthorhombic	$Pna2_1$	4.9806(3)	8.5511(6)	9.2403(6)	2.04
orthorhombic	$P2_12_12_1$	15.886(11)	11.408(4)	7.803(4)	0.26
rhombohedral	$R\bar{3}c$	4.909(2)		13.393(7)	0.52
		$GaFeO_3$			
orthorhombic	$Pna2_1$	5.0814(2)	8.7436(3)	9.3910(2)	2.74
rhombohedral	$R\bar{3}c$	5.022(2)		13.606(5)	0.14
		$Al_{0.5}Ga_{0.5}FeO_3$			
orthorhombic	$Pna2_1$	5.0306(1)	8.6461(2)	9.3175(2)	3.34
rhombohedral	$R\bar{3}c$	4.970(1)		13.509(3)	0.23

In Figure 8, we show the temperature dependence of magnetization of the $R\bar{3}c$ sample of $GaFeO_3$ under FC and ZFC conditions. There is divergence between the FC and ZFC data below 350 K, and there is no sharp ferrimagnetic transition. Thus, the magnetization curves are quite different from those of the chiral orthorhombic structure $GaFeO_3$, which shows a sharp ferrimagnetic transition at 210 K.[6,17] The magnitude of magnetization of the $R\bar{3}c$ sample is much smaller than that of the $Pna2_1$ sample showing the presence of prominent antiferromagnetic interaction. Nanoparticles of $GaFeO_3$, however, show magnetic behavior similar to that of the $Pna2_1$ $GaFeO_3$ sample but with higher T_N.

Because $AlFeO_3$ and $GaFeO_3$ show different phase-transition characteristics upon ball-milling, we have investigated the phase-transition behavior of $Al_{0.5}Ga_{0.5}FeO_3$. The structure of $Al_{0.5}Ga_{0.5}FeO_3$ under ambient conditions is the same as that of $AlFeO_3$ and $GaFeO_3$, with the space group being $Pna2_1$.[6] Upon comparison of the XRD pattern of $Al_{0.5}Ga_{0.5}FeO_3$ ($Pna2_1$) with that of the sample ball-milled for 24 h at 300 K (particle size, 25 nm), we find that the pattern of the latter is characteristic of the rhombohedral structure ($R\bar{3}c$) with lattice parameters a = 4.970(1) Å and c = 13.509(3) Å (see Figures 9 and 10). A similar change was observed after ball-milling for 6 h as well. Upon heating of the ball-milled sample to 1200 °C, it reverts back to the $Pna2_1$ structure. The Raman spectrum of the ball-milled sample of $Al_{0.5}Ga_{0.5}FeO_3$ is consistent with the $R\bar{3}c$ structure.

The magnetization behavior of $Al_{0.5}Ga_{0.5}FeO_3$ ($R\bar{3}c$) differs significantly from that of the starting $Pna2_1$ sample,[6] in that we do not see the sharp ferrimagnetic transition at 220 K. Instead, we observe divergence between FC and ZFC data below 320 K, with a narrower hysteresis at 5 K. It is interesting that partial substitution of aluminum by gallium in $AlFeO_3$ favors the direct transformation of the $Pna2_1$ phase to the $R\bar{3}c$ phase upon ball-milling without arriving at the $P2_12_12_1$ phase.

In the present study, the most significant structures encountered are the initial orthorhombic ($Pna2_1$) and the rhombohedral ($R\bar{3}c$) structures of $AlFeO_3$ and $GaFeO_3$, as shown in Figure 11. In Table 1, we list the strucural parameters of all of the phases. It is useful to discuss the structural transformation of $AlFeO_3$ in light of the various transformations of Al_2O_3.[15] The most stable structure of Al_2O_3 is the α form with the space group $R\bar{3}c$. This structure can be treated as an HCP sublattice of oxygen anions in which two-thirds of the octahedral interstices are filled with aluminum cations in an ordered array. The oxygen anions occupy 18c Wyckoff positions, the coordinates of which are x, 0, $^1/_4$ (x = 0.306), whereas the aluminum cations located at 12c positions have coordinates of 0, 0, z (z = 0.347). It has been found that Boehmite upon heating to 700 °C and above gives rise to an orthorhombic δ phase. The δ phase of Al_2O_3 is different from the δ* phase mentioned by Fargeot et al.[16] with regard to the structure of $AlFeO_3$. The δ phase derived from the spinel structure belongs to the $P2_12_12_1$ space group.[18] The orthorhombic chiral structures found by us in $AlFeO_3$ and $GaFeO_3$ are akin to the κ phase of Al_2O_3,

Table 2. Calculated Equilibrium Volumes (per Formula Unit), Binding Energies (per Formula Unit), Bulk Moduli for the Orthorhombic (Ort) and Corundum (Cor) Structures of $AlFeO_3$ and $GaFeO_3$, and Their Critical Pressures for a Transition from the Orthorhombic to Corundum Structure

compound	V(Ort) (Å^3/fmu)	V(Cor) (Å^3/fmu)	E(Ort) (eV/fmu)	E(Cor) (eV/fmu)	B(Ort) (GPa)	B(Cor) (GPa)	P_{crit} (GPa)
$AlFeO_3$	50.1	44.3	−37.59	−37.29	192	259	9
$GaFeO_3$	53.9	50.9	−33.89	−33.61	186	131.5	12.7

dx.doi.org/10.1021/ic201235h |*Inorg. Chem.* 2011, 50, 9527–9532

which has lattice parameters a = 4.69 Å, b = 8.18 Å, and c = 8.87 Å. The unit cell contains 16 cations, which are ordered in octahedral and tetrahedral sites. The packing of oxygen anions is expected to remain nearly unaffected in Al_2O_3 through the phase transformations. Chemical ordering of cations in the FCC anion structure gives rise to different structures with a partly disordered sublattice. While the orthorhombic structures are ordered, there will be considerable disorder in the $R\bar{3}c$ structure. Looking at the $Al_2O_3-Fe_2O_3$ phase diagram,[19,20] we find that at 50% composition the orthorhombic phase is stable but decomposes to the α phase of the two component oxides upon heating. In our case of phase transformation, we obtain $Pna2_1$ as the stable room temperature phase, which further transforms to the δ phase of Al_2O_3 or $R\bar{3}c$ upon ball-milling. It appears that the phase transformation is favored by disorder kinetics rather than the relative stability and pressure effects. It is to be noted in our experiment that we did not observe any decomposition of the orthorhombic $Pna2_1$ phase.

For the purpose of our calculations, we have used the lowest-energy structure of the chiral orthorhombic phase with the $Pna2_1$ space group based on our earlier work and have not considered the possibility of antisite disorder between aluminum (or gallium) and iron. On the other hand, we have considered the corundum structure ($R\bar{3}c$ space group) with half of the cation sites randomly chosen for occupation with iron because Al_2O_3 is known to take this structure and there are no distinct cation sites. We have taken into account antisite disorder in the case of the corundum structure. Our calculations of the minimum-energy volume of the crystal cell (see the results in Table 2) show that the corundum structure has a cell volume about 12 and 6% smaller than that of the orthorhombic structure of $AlFeO_3$ and $GaFeO_3$, respectively, suggesting a possible transition from the orthorhombic to corundum structure upon application of pressure. Second, the corundum structure is higher in energy than the orthorhombic one by about 0.3 eV per formula unit for both compounds. Using the minimum energies, volumes, and bulk moduli and a parabolic approximation to the energy function, our estimates of the pressure of transition from the orthorhombic to corundum structure are quite similar for both $AlFeO_3$ and $GaFeO_3$ (slightly higher for $GaFeO_3$). We should note that the critical pressure for the orthorhombic to corundum structure would reduce with disorder. We note that the estimated critical pressures for a transition from the orthorhombic to corundum structure are relatively small and readily achievable in the laboratory conditions. Before we close, we find a rather interesting coupling between magnetic ordering in the corundum structure and pressure. As the cell volume increases, our self-consistent solution reveals the development of a magnetic moment at large enough volumes (corresponding to negative pressures!) for both $AlFeO_3$ and $GaFeO_3$. While this may not be accessible directly in experiments, we believe that epitaxial films of these materials on a substrate with a larger lattice constant may favor magnetism.

Thus, the contrast between the structural behavior of $AlFeO_3$ and $GaFeO_3$ upon ball-milling cannot be explained entirely using a simple picture of pressure-induced structural phase transitions. From the results of experiments and calculations reported here, we believe that a mechanism involving an intermediate phase has to be invoked that facilitates transformation of $AlFeO_3$ from the orthorhombic phase. Because Al_2O_3 is known to occur in the δ structure with the $P2_12_12_1$ space group,[15] it is understandable why this occurs as the intermediate structure in the transformation of $AlFeO_3$.

CONCLUSIONS

The present study demonstrates how simple ball-milling can bring about interesting transformations of $AlFeO_3$ and $GaFeO_3$ from the chiral orthorhombic ($Pna2_1$) structure. This transformation in $AlFeO_3$ occurs through an intermediate $P2_12_12_1$ phase. There is an increase in the density or a decrease in the molar volume in the transformations, indicating their first-order nature. It is noteworthy that partial substitution of aluminum by gallium in $AlFeO_3$ eliminates the $P2_12_12_1$ intermediate phase. While XRD and Raman data suffice to fully characterize the phase transitions, magnetic data also throw light on the transformed phases. The phases with the $Pna2_1$ structure exhibit sharp ferrimagnetic transitions, but the $R\bar{3}c$ phases are antiferromagnetic with much smaller values of magnetization and a high irreversibility temperature. Preliminary results suggest that other properties such as the magnetodielectric characteristics are unique to the chiral orthorhombic phases of these materials. In the case of $AlFeO_3$, it is noteworthy that the orthorhombic structure seems to be more stable than the rhombohedral structure, unlike in the case of Al_2O_3.

AUTHOR INFORMATION

Corresponding Author

*E-mail: cnrrao@jncasr.ac.in. Tel: +91-80-22082761. Fax: +91-80-22082766.

REFERENCES

(1) Levine, B. F.; Nowlin, C. H.; Jones, R. V. *Phys. Rev.* **1968**, *174*, 571.
(2) Cotica, L. F.; De Medeiros, S. N.; Santos, I. A.; Paesano, A., Jr.; Kinast, E. J.; Da Cunha, J. B. M.; Venet, M.; Garcia, D.; Eiras, J. A. *Ferroelectrics* **2006**, *338*, 241.
(3) Cotica, L. F.; Santos, I. A.; Venet, M.; Garcia, D.; Eiras, J. A.; Coelho, A. A. *Solid State Commun.* **2008**, *147*, 123.
(4) Bouree, F.; Baudour, J. L.; Elbadraoui, E.; Musso, J.; Laurent, C.; Rousset, A. *Acta Crystallogr.* **1996**, *B52*, 217.
(5) Remeika, J. P. *J. Appl. Phys.* **1960**, *31*, 263S.
(6) Saha, R.; Shireen, A.; Bera, A. K.; Shirodkar, S. N.; Sundarayya, Y.; Kalarikkal, N.; Yusuf, S. M.; Waghmare, U. V.; Sundaresan, A.; Rao, C. N. R. *J. Solid State Chem.* **2011**, *184*, 494.
(7) Shireen, A.; Saha, R.; Mandal, P.; Sundaresan, A.; Rao, C. N. R. *J. Mater. Chem.* **2011**, *21*, 57.
(8) Gramsch, S. A.; Prewitt, C. T. *Spring Meeting Suppl., Abstr. M22A-07, EOS Trans. AGU* **2002**, *83*, 19.
(9) Gramsch, S. A.; Prewitt, C. T. *Fall Meeting Suppl., Abstr. MR62B-1084, EOS Trans. AGU* **2002**, *83*, 46.
(10) Nagai, T.; Hamane, D.; Devi, P. S.; Miyajima, N.; Yagi, T.; Yamanaka, T.; Fujino, K. *J. Phys. Chem. Lett. B* **2005**, *109*, 18226.
(11) Perdew, J. P.; Chevary, J. A.; Vosko, S. H.; Jackson, K. A.; Pederson, M. R.; Singh, D. J.; Fiolhais, C. *Phys. Rev. B* **1992**, *46*, 6671.
(12) Kresse, G.; Hafner, J. *Phys. Rev. B* **1993**, *47*, R558.
(13) Kresse, G.; Furthmller, J. *Phys. Rev. B* **1996**, *54*, 11 169.
(14) Kresse, G.; Joubert, D. *Phys. Rev. B* **1999**, *59*, 1758.
(15) Levin, I.; Brandon, D. *J. Am. Ceram. Soc.* **1998**, *81*, 1995.
(16) Fargeot, D.; Mercurio, D.; Dauger, A. *Mater. Chem. Phys.* **1990**, *24*, 299.
(17) Frankel, R. B.; Blum, N. A.; Foner, S.; Freeman, A. J.; Schieber, M. *Phys. Rev. Lett.* **1965**, *15*, 958.
(18) Bonevich, J. E; Marks, L. D *J. Mater. Res.* **1992**, *7*, 1489.
(19) Levi, C. G. *Acta Mater.* **1998**, *46*, 787.
(20) Polli, A. D.; Lange, F. F.; Levi, C. G *J. Am. Ceram. Soc.* **1996**, *79*, 1745.